Journal of Materials Chemistry A

c8ta04077j

50

We have presented the Graphical Abstract text and image for your article below. This brief summary of your work will appear in the contents pages of the issue in which your article appears.

PAPER 1 1 Nanoporous gyroid Ni/NiO/C nanocomposites from 5 5 block copolymer templates with high capacity and Removal of PS stability for lithium storage Nanoporous gyroid Ni/NiC Chung-Fu Cheng, Yu-Ming Chen, Feng Zou, Kai-Chieh Yang, Tzu-Ying Lin, Kewei Liu, Chi-Huang Lail Rong-Ming Ho* and Yu Zhu* 10 10 Nanoporous gyroid Ni/NiO/C nanocomposite electrodes Nanoporous gyroid Ni/NiO/C exhibited good cycling stability over 1000 cycles at 1 A $\rm q^{-1}$ with a specific capacity of 800 mA h g⁻¹ 15 15 Please check this proof carefully. Our staff will not read it in detail after you have returned it. Proof corrections must be returned as a single set of corrections, approved by all co-authors. No further corrections can be 20 20 made after you have submitted your proof corrections as we will publish your article online as soon as possible after they are received. Please ensure that: 25 25 The spelling and format of all author names and affiliations are checked carefully. Names will be indexed and cited as shown on the proof, so these must be correct. Any funding bodies have been acknowledged appropriately. All of the editor's queries are answered. 30 30 Any necessary attachments, such as updated images or ESI files, are provided. Translation errors between word-processor files and typesetting systems can occur so the whole proof needs to be read. Please pay particular attention to: tables; equations; numerical data; figures and graphics; and references. 35 35 Please send your corrections preferably as a copy of the proof PDF with electronic notes attached or alternatively as a list of corrections – do not change the text within the PDF file or send a revised manuscript. Corrections at this stage should be minor and not involve extensive changes. Please return your final corrections, where possible within 48 hours of receipt, by e-mail to: materialsA@rsc.org. If you require 40 40 more time, please notify us by email. 45 45

Funder information

Providing accurate funding information will enable us to help you comply with your funders' reporting mandates. Clear acknowledgement of funder support is an important consideration in funding evaluation and can

increase your chances of securing funding in the future. We work closely with Crossref to make your research discoverable through the Funding Data search tool (http://search.crossref.org/funding).

Further information on how to acknowledge your funders can be found on our webpage (http://rsc.li/funding-info).

10 What is Funding Data?

10

Funding Data (http://www.crossref.org/fundingdata/) provides a reliable way to track the impact of the work that funders support. We collect funding information from our authors and match this information to funders listed in the Crossref Funder Registry. Once an article has been matched to its funders, it is discoverable through Crossref's search interface

15

1

5

PubMed Central

15

20

30

35

40

45

55

П

Accurate funder information will also help us identify articles that are mandated to be deposited in PubMed Central (PMC) and deposit these on your behalf.

20

Providing funder information

We have combined the information you gave us on submission with the information in your acknowledgements. 25 This will help ensure funding information is as complete as possible and matches funders listed in the Crossref Funder Registry. Please check that the funder names and grant numbers in the table are correct. This table will not be included in your final PDF but we will share the data with Crossref so that your article can be found via the Funding Data search tool.

25

Funder name	Funder ID (for RSC use only)	Award/grant/contract number	
Division of Materials Research	10000078	1554851	
Division of Chemical, Bioengineering, Environmental, and Transport Systems	100000146	1505943, 1706681	3.
University of Akron	100008875	Unassigned	
National Science Foundation	10000001	NSF-CBET1505943, 1706681, NSF-DMR1554851	4

If a funding organisation you included in your acknowledgements or on submission of your article is not currently listed in the registry it will not appear in the table above. We can only deposit data if funders are already listed in the Crossref Funder Registry, but we will pass all funding information on to Crossref so that additional funders can be included in future.

45

Researcher information

If any authors have ORCID or ResearcherID details that are not listed below, please provide these with your proof 50 corrections.

50

Please check that the ORCID and ResearcherID details listed below have been assigned to the correct author. Authors should have their own unique ORCID iD and should not use another researcher's, as errors will delay publication.

55

Please also update your account on our online manuscript submission system to add your ORCID details, which will then be automatically included in all future submissions. See here for step-by-step instructions and more information on author identifiers.

1	First (given) name(s)	Last (family) name(s)	ResearcherID	ORCID	1
	Chung-Fu	Cheng			
5	Yu-Ming	Chen			
	Feng	Zou			5
	Kai-Chieh	Yang			
	Tzu-Ying	Lin			
	Kewei	Liu			10
	Chi-Huang	Lai		0000-0002-9250-0015	
	Rong-Ming	Но			
15	Yu	Zhu		0000-0002-2201-9066	15
20					20
25					25
30					30
35					35
40					40
45					45
50					50
55					55

Queries for the attention of the authors 1 Journal: Journal of Materials Chemistry A 5 Paper: c8ta04077j Title: Nanoporous gyroid Ni/NiO/C nanocomposites from block copolymer templates with high capacity and stability for lithium storage For your information: You can cite this article before you receive notification of the page numbers by using the 10 10 following format: (authors), J. Mater. Chem. A, (year), DOI: 10.1039/c8ta04077j. Editor's queries are marked on your proof like this 1, 2, etc. and for your convenience line numbers are indicated like this 5, 10, 15, Please ensure that all queries are answered when returning your proof corrections so that publication of your 15 15 article is not delayed. Query Querv Remarks Reference 20 20 Funder details have been incorporated in the funder table using OK 1 information provided in the article text. Please check that the funder information in the table is correct. Please confirm that the spelling and format of all author names is One coauthor's name should 25 25 2 correct. Names will be indexed and cited as shown on the proof, be changed, see comments so these must be correct. No late corrections can be made. The sentence beginning "With the increased energy ..." has been 3 OK altered for clarity. Please check that the meaning is correct. 30 30 The caption to Fig. 3 refers to part (g) but the image as supplied (g) should be (f), (f) should be (e) see comments in email does not contain a part labelled (g). Would you like to modify the 4 caption or resupply the artwork (preferably as a TIF file at 600 dots per inch)? The sentence beginning "Following the fabrication of..." has been 35 35 5 OK altered for clarity. Please check that the meaning is correct. The sentence beginning "The Ni/NiO composite..." has been highlighted words should be 6 altered for clarity. Please check that the meaning is correct. changed to "a calcination process was performed to 40 40 remove the PS template and oxidize Ni" 45 45

ART ■ C8TA04077J_GRABS

50

55

50

Journal of Materials Chemistry A



PAPER

1

5

Cite this: DOI: 10.1039/c8ta04077j

1

5

10

15

20

25

30

35

40

45

50

Nanoporous gyroid Ni/NiO/C nanocomposites

10

15

25

30

35

40

45

Received 3rd May 2018 Accepted 14th June 2018

20 DOI: 10.1039/c8ta04077j

rsc.li/materials-a

from block copolymer templates with high capacity and stability for lithium storage†

Chung-Fu Cheng,^a Yu-Ming Chen,^a Feng Zou,^a Kai-Chieh Yang,^b Tzu-Ying Lin,^c Kewei Liu, a Chi-Huang Lai, Rong-Ming Ho*b and Yu Zhu 10 ka

A nanoporous Ni/NiO/C nanocomposite with a gyroid nanostructure was fabricated by using a nanoporous polymer with gyroid nanochannels as a template. The polymer template was obtained from the selfassembly of a degradable block copolymer, polystyrene-b-poly(L-lactide) (PS-PLLA), followed by the hydrolysis of PLLA blocks. Templated electroless plating followed by calcination was performed to create a precisely controlled Ni/NiO gyroid nanostructure. After carbon coating, a well-interconnected nanoporous gyroid Ni/NiO/C nanocomposite can be successfully fabricated. Benefiting from the wellinterconnected nanoporous structure with ultrafine transition metal oxide and uniform carbon coating, the gyroid nanoporous Ni/NiO/C nanocomposite electrodes exhibited high specific capacities at various rates (1240 mA h g^{-1} at 0.2 A g^{-1} , 902 mA h g^{-1} at 2 A g^{-1} and 424 mA h g^{-1} at 10 A g^{-1}) and excellent cyclability (809 mA h g^{-1} at 1 A g^{-1} after 1000 cycles, average coulombic efficiency 99.86%). This research demonstrates a universal approach for constructing a nanostructured electrode with explicitly controlled block copolymer phase separation.

1 Introduction

B With the increased energy demand from the emerging technologies such as wearable electronics and electric-powered vehicles, various functional high-efficiency energy storage devices have attracted extensive attention in recent years. 1-6Among the electrochemical energy storage devices, lithium ion batteries (LIBs) are highly desirable in portable electronic devices as well as greener automobiles, including electric vehicles (EVs) and hybrid electric vehicles (HEVs).7-12 Nevertheless, a commercial graphite anode exhibits a relatively low theoretical specific capacity of 372 mA h g^{-1} , which is no longer able to fulfill the requirements of emerging applications such as EVs, where higher energy density and power density are of paramount importance. In order to increase the energy density and power density of LIBs, novel anode nanomaterials with lower cost, higher specific capacity, and better durability as well as ratability are urgently needed. Transition metal oxides (MO_x, M = Mn, Fe, Ni, Co, Sn, etc.), as emerging conversion-reaction

type anode materials, are appealing candidates due to their higher specific capacities (\sim 1000 mA h g⁻¹) compared to that of an intercalation anode like graphite.13-19 Furthermore, within the transition metal oxide category, nickel oxide-based nanomaterials are one of the most studied systems due to their high lithium storage capacity.20-25 However, the performance of the nanostructured NiO anode has been limited by its poor electrical conductivity and large volume variation upon lithiation and de-lithiation. 26,27 Various methods have been carried out to accommodate the volume expansion phenomenon and enhance the electrical conductivity. For instance, successful nanostructure engineering of transition metal oxide materials has been demonstrated in lithium ion batteries14,28-30 to mitigate the volume-change-induced mechanical strain. Additionally, hybridization with carbonaceous materials (graphene, graphene oxides, carbon nanotubes, or conductive polymers) has been used to enhance the conductivity of the transition metal oxide electrode.31-34Another straightforward route to fabricate nanostructured NiO with carbonaceous hybrid materials is to directly deposit desired NiO-based materials into templates with defined nanochannels through templated syntheses using nanostructured carbon or a nanoporous polymer as a template.35-38

In recent decades, block copolymers (BCPs) have been comprehensively investigated because of their capability to selfassemble into one-, two-, and three-dimensional periodic nanostructures while being readily adjustable in size, which is dependent on their constituted compositions and molecular

^aDepartment of Polymer Science, University of Akron, Akron, Ohio 44325, USA. E-mail: yu.zhu@uakron.edu

^bDepartment of Chemical Engineering, National TsingHua University, Hsinchu 30010,

^{&#}x27;Department of Materials Science and Engineering, National TsingHua University, Hsinchu 30010, Taiwan

[†] Electronic supplementary information (ESI) available. 10.1039/c8ta04077i

15

20

35

40

55

1

5

10

15

20

30

35

weights.^{39,40} Moreover, the degradable characteristic of BCPs is advantageous because it enables the synthesis of nanoporous polymers with a well-ordered texture by simple removal of degradable component(s) in BCPs through hydrolysis,^{41–43} ozonolysis,⁴⁴ UV degradation,⁴⁵ reactive ion etching⁴⁶ or hydrofluoric acid etching.⁴⁷ In addition, the nanoporous polymers with well-defined nanochannels, in particular, for the gyroid-structured phase from the self-assembly of BCPs, can be used as templates for templated synthesis.⁴⁸ By exploiting the templating process, reactions such as atomic layer deposition,^{49,50} electrochemical deposition,^{51–53} electroless plating,^{54–57} and solgel reaction^{58–60} can be carried out using the BCP templates for the fabrication of nanoporous inorganic materials with precisely controlled morphology after removal of the polymer template.

Herein, a new approach is proposed for the fabrication of the nanoporous gyroid Ni/NiO/C nanocomposite with a welldefined morphology (i.e., gyroid-forming nanostructure). The well-ordered network structures are of particular interest as they exhibit excellent performance in mitigating the volume expansion.61 The continuous gyroid structure also provides an ideal electron transport channel (through the structure of gyroid itself) and an ion transport channel (through the continuous voids of the gyroid matrix) for the electrode, enhancing the power of the electrode. The nanoporous gyroid nanocomposite was synthesized by using hydrolyzed polystyrene-b-poly(L-lactide) (PS-PLLA) to prepare the nanoporous PS template with gyroid-forming nanochannels, 54-60 followed by templated electroless plating of Ni to form PS/Ni nanohybrids. In order to convert the Ni-based gyroid structure into a conductive electrode material, a modified two-step calcination process was incorporated in this study. The main purpose is to thermally decompose the PS template with good preservation of the gyroid structure and to post oxidize the Ni into NiO. It must be noted that severe collapse may occur if the PS template is drastically removed. Therefore, it is necessary to attune the ramping temperature process for removal of the PS template and oxidation of Ni, in order to prevent the drastic deformation of the nanostructure. After removal of the PS template and further oxidation of Ni, a subsequent carbon coating procedure was performed to enhance the conductivity. This nanoporous gyroid-structured Ni/NiO/C nanocomposite is an ideal anode material for the highperformance lithium-ion battery as it possesses a well-interconnected nanoporous structure with an ultrafine transition metal oxide nanonetwork and uniform carbon coating. These desirable features enable the subsequently fabricated electrodes to exhibit high specific capacity while simultaneously providing excellent electrical conductivity and a robust structure. Consequently, the LIB with this novel anode exhibits an extremely long cycle life of 1000 cycles at a current density of 1 A g⁻¹ and excellent rate performance. To the best of our knowledge, the Ni/NiO/C nanocomposite with a wellordered unique nanoporous gyroid structure serving as an anode in LIB, giving such outstanding performance and cyclability, has not been previously reported.

2 Experimental section

Synthesis of PS-PLLA

Detailed synthetic strategy and routes for the PS-PLLA sample were described in previously published results. ^{54,55} Generally, PS-PLLA was synthesized by atomic transfer radical polymerization (ATRP) using a double-headed initiator. GPC was further utilized to characterize the number-average molecular weight and polydispersity index (PDI) of the product. The PDI of the synthesized PS-PLLA was then further determined and the repeated unit number of L-LA *versus* PS was determined by ¹HNMR analysis. In this study, the number-average molecular weights of PS and PLLA and the PDI of PS-PLLA are 34 000 g mol⁻¹, 27 000 g mol⁻¹ and 1.21, respectively. For the given densities of PS and PLLA (1.02 and 1.248 g cm⁻³, respectively), the volume fraction of PLLA, $f_{\rm PLLA}$, is then calculated as 0.37.

Preparation of the block copolymer template

Solution casting was carried out to prepare bulk samples of PS-PLLA with dichloromethane (CH₂Cl₂) as solvent (10 wt% of PS-PLLA) at room temperature. The samples were set for two weeks, and then dried in a vacuum oven at 65°C for three days. With an aim to eliminate the residual PLLA crystals, the dried samples were heated to the maximum annealing temperature, $T_{\text{max}} =$ 175°C for 3 minutes. After quenching (by using liquid nitrogen) the microphase-separated ordered melt at 175°C, the samples were used for SAXS experiments. To prepare the nanoporous PS template with the gyroid nanochannel, hydrolysis of PLLA blocks from the PS-PLLA samples was carried out by using a 0.5 M basic solution that was prepared by dissolving 2 g of sodium hydroxide in a 40/60 (by volume) solution of methanol/ water. After three days of hydrolysis to complete the removal of PLLA, the hydrolyzed samples were rinsed with a mixture of DI water and methanol, and then used as templates for following experiments.

Templated electroless plating of Ni

The nanoporous PS templates with interconnected air networks were soaked in seeding aqueous solution mixed with methanol (12 ml) and PdCl₂ (0.01-0.02 g) with stirring at room temperature for 3-4 hours. After washing gently with methanol/H₂O solution to remove redundant Pd ions covering on sample surfaces, the pore-filled samples were immersed into a hydrazinium hydroxide (85%, 4 ml) methanol solution for the nucleation of Pd. With the control of low enough Pd ion concentrations, a suitable amount of Pd nuclei within the nanochannels of the template can be formed. Subsequently, a fresh aqueous solution consisting of NiCl2 (0.4 g), hydrazinium hydroxide (4 ml), ammoniumhydroxide (6.4 ml), DI water (40 ml) and methanol (40 ml) was prepared and then the pretreated templates with low content of Pd nuclei were immersed into the prepared solution. Accordingly, Ni ions were reduced to Ni clusters arising from preformed Pt nuclei so as to gradually develop within the nanochannels throughout the growth process and eventually form the PS/Ni nanohybrids with a preserved gyroid texture.

5

20

35

40

45

10

15

20

25

30

35

40

45

50

55

Formation of the nanoporous gyroid Ni/NiO nanocomposite

To produce the nanostructured Ni/NiO nanocomposite, the PS template of the PS/Ni nanohybrids was degraded and oxidized by modified calcination under air purge. The temperature was first increased to 350°C and kept for 1 h for further stabilization. After that, the temperature was then increased to 450°C. Finally, the temperature was further kept at 550°C for 5 h to complete the PS removal. In the second oxidation stage, the temperature was then decreased to 450°C and stabilized for 1 h. After that, the temperature was decreased to 350°C for 1 h and then decreased to room temperature. Consequently, the nanostructured Ni/NiO materials were obtained.

Carbon coating

Carbon coating was performed by atmospheric pressure chemical vapor deposition (CVD). Acetylene was used as the carbon source and the reaction temperature was 450° C. A continuous argon purge was used during the carbon coating process. The sample was loaded in a ceramic boat and the coating time is 5 min. The flow rates of acetylene and argon were 4 and 200 sccm, respectively.

Battery fabrication

The nanoporous gyroid Ni/NiO/C nanocomposite was mixed with carbon black and PAA at a weight ratio of 7:2:1, respectively. The addition of NMP and subsequent mixing using a pestle and mortar produced a homogenous thick slurry. The mixture slurry was cast on copper foil using a doctor blade. The cast electrode was placed in a vacuum oven at 50°C overnight to remove solvent. 2032 coin cells were used for the fabrication of half cells. The fabrication of the cells was conducted in an Ar glovebox. Lithium metal was used as the counter electrode and Celgard 3501 as the separator. The electrolyte is 1 M lithium hexafluorophosphate solution in EC and DEC (1:1 v/v) with 10 wt% fluoroethylene carbonate. The electrodes were punched into 5/16 circular discs, typically with a mass loading of 0.4–0.6 mg cm⁻².

3 Results and discussion

The fabrication procedure of the Ni/NiO/C nanocomposite with a nanoporous gyroid structure is illustrated in Fig. 1. A PS-PLLA

sample with a molecular weight of 61 000 g mol⁻¹ and a PLLA volume fraction of 37% was synthesized, following the previous reports.^{37,38} A gyroid-forming phase consisting of co-continuous PLLA networks in a PS matrix can be formed after solution casting of the synthesized PS-PLLA followed by quenching from the microphase-separated melt. The one-dimensional smallangle X-ray scattering (1D SAXS) profile (curve (i) in Fig. 2(a)) confirms the formation of a gyroid phase from the self-assembly of PS-PLLA at which reflections are found at the relative q values of $\sqrt{6}$: $\sqrt{8}$: $\sqrt{14}$: $\sqrt{16}$: $\sqrt{32}$. The inter-domain spacing of the $(211)_{\text{evroid}}$ $(d_{(211)G})$ was determined as approximately 51.2 nm from the primary reflection, suggesting a cubic unit cell of 119.7 nm for the forming gyroid phase. Fig. 2(a) displays the 1DSAXS profile of PS-PLLA after hydrolysis (curve (ii)); the reflections at the relative q values remain unchanged as compared to curve (i) in Fig. 2(a), reflecting the preservation of the gyroid phase after hydrolytic treatment, suggesting that the PLLA networks can be selectively removed. As a result, the PS matrix with well-defined, bi-continuous nanochannels can be fabricated, and then employed as a template for following electroless plating of Ni. The corresponding one-dimensional wide-angle X-ray diffraction (1D XRD) profile shown in Fig. S1(c)† confirmed the formation of Ni in the PS matrix.

To acquire high conversion of Ni to NiO, a 2nd stage calcination was conducted by controlling the treatment temperature (from 550°C to room temperature), the diffusion of oxygen into nanoporous Ni will occur after removal of the PS template, giving rise to the acquired degree of thermal oxidation of Ni. As shown in Fig. 3(a), all the diffractions can be indexed as fcc (both Ni and NiO) based on JCPDS card no. 04-0850 and no. 47-1049, respectively. The lattice constant was calculated by the first diffraction peak with $a_{Ni} = 3.520 \text{ Å}$ and $a_{NiO} = 4.171 \text{ Å}$. Note that all diffractions can be well indexed as the reflections of (111) and (200) for Ni, and (111), (200) and (220) for NiO, suggesting that the nanoporous gyroid Ni/NiO nanocomposite can be trustfully fabricated after the designed thermal processes for calcination. As shown in Fig. 3(b), the FESEM micrograph depicts the unique gyroid texture with tripod and three-fold symmetry after the calcination, indicating that the well-ordered nanonetwork for the nanoporous gyroid NiO/Ni nanocomposite was successfully fabricated. High-resolution TEM (HRTEM) was utilized to prove the crystalline lattice in real space. Fig. 3(d) displays the lattice fringes of Ni and NiO grains. The (111) and



Fig. 1 Schematic illustration of fabricating a nanoporous gyroid Ni/NiO/C nanocomposite using a polymer template from self-assembled degradable BCPs: (a) nanoporous gyroid PS; (b) PS/Ni nanohybrids via templated electroless plating; (c) removal of PS and oxidation of Ni with controlled calcination. (d) Nanoporous gyroid Ni/NiO/C nanocomposite after carbon coating.

Journal of Materials Chemistry A Paper

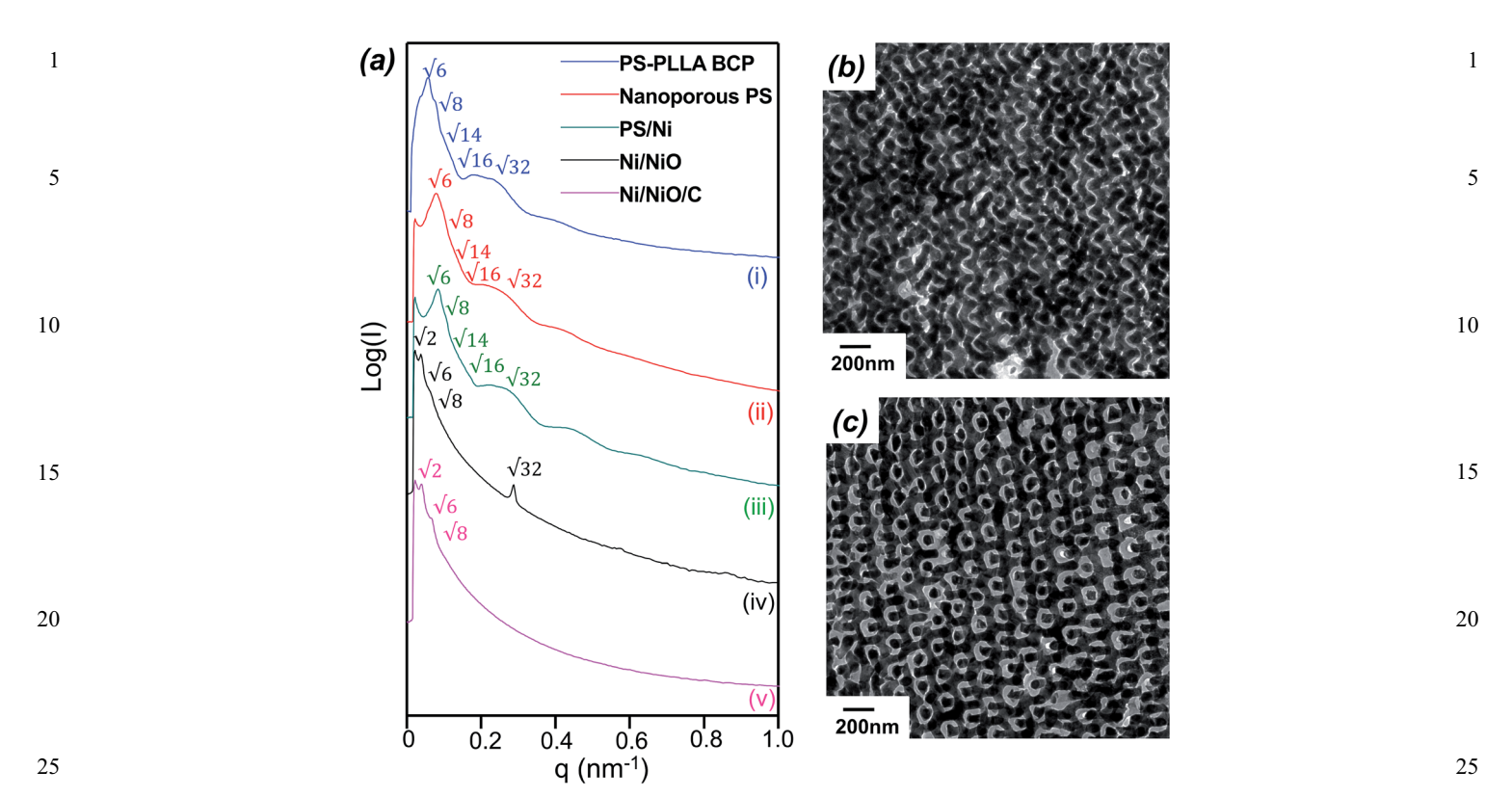


Fig. 2 Nanostructural characterization. (a) 1D Small angle X-ray scattering (SAXS) profiles of (i) self-assembled PS-PLLABCPS; (ii) nanoporous PS template after removal of the PLLA blocks in PS-PLLABCP by hydrolysis; (iii) PS/Ni gyroid-structured nanohybrids; (iv) nanoporous gyroid Ni/NiO nanocomposite; (v) nanoporous gyroid Ni/NiO/C nanocomposite. (b) TEM micrographs of the PS/Ni nanohybrids with projection planes along the [211] direction of the gyroid structure. (c) TEM micrographs of the PS/Ni nanohybrids with projection planes along the [100] direction of the gyroid structure. The dark contrast represents Ni while the white contrast represents PS.

(200) reflections of Ni and the (200) reflection of NiO (Fig. 3(e and f)) are in line with the calculated results from XRD (Fig. 3(a)). Also, Fig. 3(f) shows a clear interface between Ni and NiO, suggesting the formation of the Ni/NiO nanocomposite. Furthermore, X-ray photoelectron spectroscopy (XPS) was used to examine the elemental composition of the nanoporous gyroid Ni/NiO nanocomposite (Fig. S4†). The results also confirmed that significant oxygen content was observed. As a result, the degeneration of the PS template and the thermal oxidation of Ni should be successfully achieved by the designed thermal processes for calcination to give the nanoporous gyroid Ni/NiO nanocomposite. The structure of the nanoporous gyroid Ni/NiO nanocomposite can be further identified by SAXS (curve (iv) in Fig. 2(a)); the reflections at the relative q values of $\sqrt{2}$: $\sqrt{6}$: $\sqrt{8}$: $\sqrt{32}$ can be found. Note that the appearance of the $\sqrt{2}$ peak is attributed to the formation of network shifting resulting from removal of the PS template, giving single gyroid like scattering with reflections similar to the space group of *I*4₁32.^{58,62} Although the characteristic reflections for the samples containing Ni/NiO at high q range are relatively broad, the identification of the gyroid nanostructure can be verified by corresponding SAXS results consisting of the reflections at a q ratio of $\sqrt{2}$ and $\sqrt{6}$.

Carbon coating has been proved as an effective method to improve the stability of the nanomaterial electrode. ^{32,53,63} With conformal carbon coating, the electrode made from this

conversion reaction material will not only have high specific capacity but also possesses a stable SEI layer, excellent electrical conductivity, and a robust structure. To fulfill the requirement of the high stability of the nanoporous gyroid Ni/NiO nanocomposite fabricated, carbon coating was performed to fabricate the nanoporous gyroid Ni/NiO/C nanocomposite via chemical vapor deposition (CVD) using acetylene as the carbon source (see ESI† for details). As shown in Fig. 3(c), the FESEM micrograph displays the nanostructure of the nanoporous gyroid Ni/NiO/C nanocomposite after carbon coating. The structure of the nanoporous gyroid Ni/NiO/C can be further identified by SAXS (curve (v) in Fig. 2(a)); the reflections at a qratio of $\sqrt{2}$ and $\sqrt{6}$ can be verified, suggesting that the wellordered nanonetworks with a gyroid structure can be wellpreserved after the carbon coating. The forming nanonetworks can be in a long-range order as shown in Fig. S5† for the FESEM observation at low magnification. Also, the nitrogen adsorption/ desorption isotherm at 77 K was performed to investigate the specific surface area of the nanoporous gyroid Ni/NiO/C nanocomposite. As shown in Fig. S6(a),† the nanoporous gyroid Ni/ NiO/C nanocomposite shows a Brunauer-Emmett-Teller (BET) specific surface area of approximately 18.7 m² g⁻¹. As confirmed by the pore size distribution (Fig. S6(b)†), the corresponding average pore size was about 18.8 nm.

30

35

40

55

Furthermore, as evidenced by the WAXD (Fig. 3(a)), the forming NiO can be well preserved after the formation of carbon

30

35

40

50

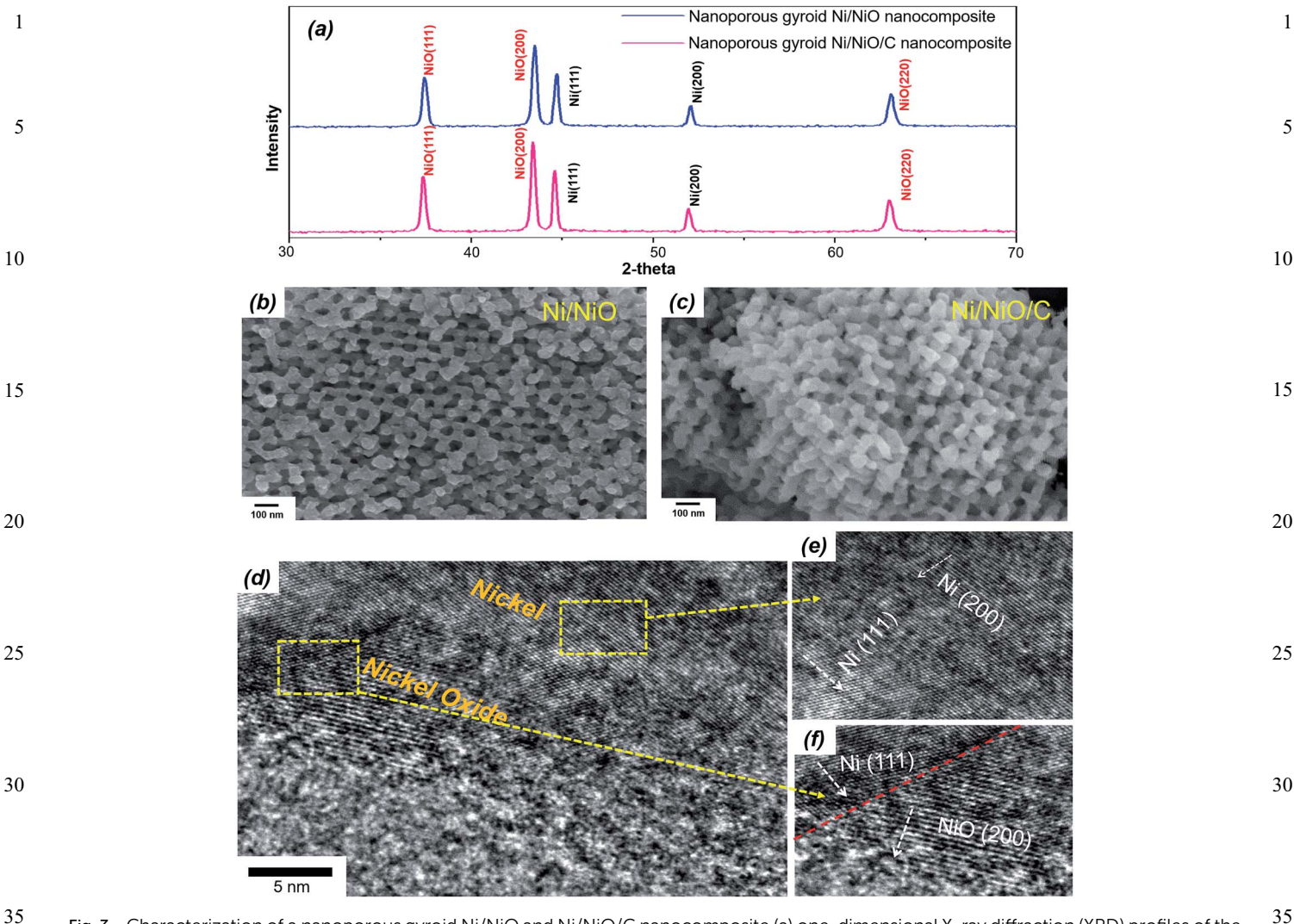


Fig. 3 Characterization of a nanoporous gyroid Ni/NiO and Ni/NiO/C nanocomposite (a) one-dimensional X-ray diffraction (XRD) profiles of the nanoporous gyroid NiO/Ni nanocomposite and Ni/NiO/C nanocomposite; the diffraction peaks of Ni are indexed as black while the peaks of NiO are indexed as red. (b and c) Field emission scanning electron microscope (FESEM) micrographs of the nanoporous gyroid Ni/NiO nanocomposite (b) Ni/NiO/C nanocomposite after carbon coating (c). (d-f) HRTEM micrographs of the nanoporous gyroid Ni/NiO nanocomposite. (f) The enlarged area shows the lattice fringes and the arrows show the directions for the grains of the Ni and (g) shows the interface of Ni and NiO.

coating at which the diffraction peaks of NiO remain unchanged. XPS was used to examine the elemental composition of the nanoporous gyroid Ni/NiO/C nanocomposite (Fig. S7†). As validated by the Ni 2p XPS results (Fig. S8(a)†), four peaks are displayed: $2p_{3/2}$ (854.9 eV and 862.1 eV) as well as $2p_{1/2}$ (873.3 eV and 880.1 eV). Compared with previous XPS results of NiO⁶⁴ and Ni(OH)₂,⁶⁵ it was concluded that the surface of materials could be Ni(OH)2 coated NiO.66 Since the formation of NiO is through the oxidation by oxygen in air, it is expected that NiO instead of Ni is detected by a surface characterization method like XPS. However, XRD results indicated that majority of the materials are NiO and Ni. The Ni(OH)₂ detected from XPS could have resulted from the hydrolyzation of samples during the short exposure to air. The value of the binding energy difference between Ni $2p_{3/2}$ and Ni $2p_{1/2}$ is about 18.4 eV, which reveals the presence of NiO.67,68 The formation of C and O characteristic peaks after the carbon coating is displayed in

Fig. S8(b) and (c),† reflecting that the nanoporous Ni/NiO/C nanocomposite can be well prepared. The composition of C and NiO of the nanoporous gyroid Ni/NiO/C nanocomposite was determined by thermogravimetric analysis (TGA) (Fig. S9†). On the basis of the TGA result, the compositions of Ni, NiO and C are about 13%, 74% and 13%, respectively. Such a thin, conformal carbon coating is of pivotal importance for lithium ion batteries (LIB) because it not only provides high conductivity for the transition metal network but also improves the formation of a stable SEI layer, without sacrificing a significant amount of capacity.²¹

Electrochemical properties of a nanoporous gyroid Ni/NiO/C nanocomposite anode: to systematically investigate the electrochemical performance of the nanoporous gyroid Ni/NiO/C nanocomposite, LIB half cells using the nanoporous gyroid Ni/NiO/C nanocomposite and a lithium metal counter electrode were fabricated. Cyclic voltammetry (CV) measurement was

50

55

40

45

50

Journal of Materials Chemistry A

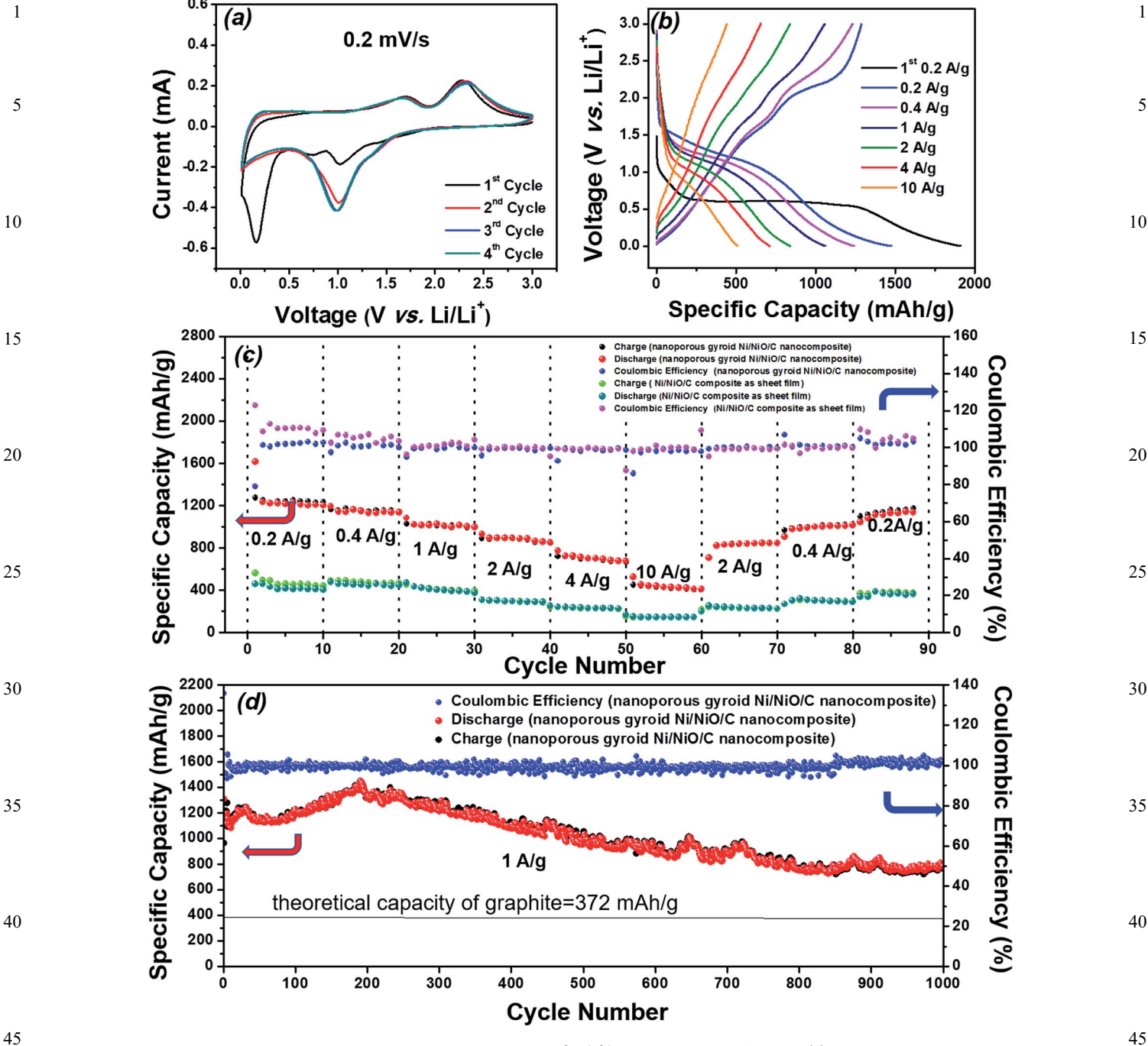


Fig. 4 Electrochemical performance of the nanoporous gyroid Ni/NiO/C nanocomposite for LIBs (a) cyclic voltammogram curves of the nanoporous gyroid Ni/NiO/C nanocomposite anode collected at the scan rate of $0.2~\text{mV}~\text{s}^{-1}$ within the voltage range of 0.005-3~V. (b) Charge/discharge profiles at different current densities of 0.2, 0.4, 1.2,

performed under a scan rate of 0.2 mV s^{-1} within the voltage range of $0.005\text{--}3 \text{ V} \nu s$. Li/Li⁺. Fig. 4(a) depicts the first four cycles of the cyclic voltammetry (CV). In the first cathodic process, the peak at 0.2 V is attributed to the formation of the SEI film and the reduction of NiO to metallic Ni, and the peak at 1.0 V can be

attributed to the generation of Li₂O. There are two broad oxidation peaks in the following anodic process; the one at 2.2 V is due to the reversible oxidation of Ni to NiO (Ni + Li₂O \rightarrow NiO + 2Li⁺ + 2e⁻), and the other at 1.7 V is caused by the partial decomposition of SEI components.⁶⁸ The overall electrochemical reaction of

50

55

50

10

15

20

35

40

45

55

20

45

the nanoporous gyroid Ni/NiO/C nanocomposite electrode can be described using the following equation:

$$NiO + 2Li^+ + 2e^- \Leftrightarrow Ni + Li_2O$$
 (1)

In the subsequent cycles, reduction peaks shift to about 1.1 V and oxidation peaks slightly shift to about 2.3 V and 1.6 V. These two redox reactions of lithium ions with the electrode are highly reversible. The difference between the equivalent peaks in the first cycle and subsequent cycles can be ascribed to the formation of the SEI layer on the carbon surface. 69,70

Fig. 4(b) shows the representative discharge–charge profiles of the nanoporous gyroid Ni/NiO/C nanocomposite electrode at various current densities. The electrode exhibits a potential plateau at 0.7 V during the first discharge (0.2 A g^{-1}). After the first cycle, this long potential plateau is replaced by a longsloped curve from 1.7 to 0.9 V, which is a typical phenomenon observed in the conversion reaction electrode. In addition, the first discharge and charge profile delivered specific capacities of 1754 and 1240 mA h g⁻¹, respectively. The capacity loss of 29.3% is mainly attributed to the interfacial reaction between NiO and the electrolyte. 18,22,24 As expected, the increase in current density gives rise to higher overpotential, resulting from the kinetic effects of the electrode materials, in terms of lower discharge plateau and higher charge potential. However, the discharge and charge curves under different rates still display a similar curve shape. The nanoporous gyroid Ni/NiO/C nanocomposite electrode also exhibits an impressive rate capability. Fig. 4(c) shows the rate capability behavior over 90 cycles from 0.2 A g^{-1} to 10 A g^{-1} . The discharge specific capacities are 1242, 1154, 1023, 902, 674 and 424 mA h g⁻¹ at 0.2, 0.4, 1, 2, 4 and 10 A g⁻¹, respectively. Notably, even after cycling at a relatively high current density at 10 A g^{-1} (i.e., C rate = 14C), the capacity can recover in proximity to its corresponding value when the current density is set back to 2 A g⁻¹ and 0.4 A g⁻¹. Furthermore, when the current density is set back to the initial rate (0.2 A g^{-1}) , the capacity can almost recover to the original value (i.e., the specific capacity is 1214 mA h g⁻¹ for recovery cycle). Notably, in contrast to the reported results of the NiO-based electrode, 20-24 the nanoporous gyroid Ni/NiO/C nanocomposite exhibits better rate performance (Fig. S10†). It is worth noting that the specific capacity achieved here is even higher than the theoretical capacity of NiO (718 mA h g^{-1}) based on the conversion reaction mechanism. We believe that the additional capacity was achieved through the lithium storage on the nanoscale interface and partially reversible SEI decomposition.71 The gyroid nanostructure would be an ideal case for the lithium storage in the nanoscale interface, which is also observed in previous reports where the nanoporous transition metal oxide electrodes were used.20,23 The oxidation peak at 1.6 V from CV of the anode (Fig. 4(a)) corresponds to partial decomposition of the anode.²¹ To further understand the enhancement in specific capacity from the gyroid nanostructure, Ni/NiO/C composite materials with sheet-film morphology (see ESI for detailed preparation†) were also prepared and characterized (Fig. S11(a and b)†). The sheet-film Ni/NiO/C composite materials were tested in the batteries as well and the results are shown in Fig. 4(c) and S11(c, d).† As shown in Fig. 4(c), the rate performance indicated that the random structured Ni/NiO/C sheet-film composite anode exhibited significantly lower specific capacity as compared to the nanoporous gyroid Ni/NiO/C nanocomposite anode under all current densities, particularly at high C-rate cycles. We speculate that the excellent rate capability performance of the nanoporous gyroid Ni/NiO/C nanocomposite is attributed to the bicontinuous nature of the gyroid structure that provides both short lithium diffusion distance and ideal electron transport paths.

The cycling performance of the nanoporous gyroid Ni/NiO/C nanocomposite anodes was further investigated. The data shown in Fig. 4(d) were recorded at 0.2 A g⁻¹ for the initial four cycles to fully activate the electrode, and then the data were collected at 1 A g⁻¹ current density for the following cycles in the voltage range of 0.02-3.0 V (vs. Li/Li⁺). The nanoporous gyroid Ni/NiO/C nanocomposite electrode exhibited excellent cycling stability with a capacity steadily increasing up to 1446 mA h g^{-1} after 191 cycles from the initial value of 1151 mA h g^{-1} . Furthermore, the rise in capacity was elucidated by the changes in capacity plateaus of the 60th, 90th, 120th, 150th and 180th cycles as shown in Fig. S12.† The rise in capacity is not surprising for the nanostructured NiO-based electrode. This is usually explained by the gradual amorphization of crystalline NiO, which produces more Li ion accessible sites and improves kinetics for reoxidation of Ni to NiO. 22,72 The electrochemical impedance analysis of the nanoporous gyroid Ni/NiO/C nanocomposite electrode (see ESI, Fig. S13†) was conducted during the long cycle test. As shown in Fig. S13,† the EIS of the initial anode and the anode after 100, 400 and 800 cycles was presented. An equivalent circuit displayed in the inset of Fig. S13 \dagger was used to fit the spectra. The R_s represents the intrinsic resistance of the active materials, electrolyte and ionic resistance. The R_{sf} and CPE_{sf} relate to the resistance and the constant phase element of the SEI film, respectively; while the resistance and the constant phase element of the charge transfer are denoted as R_{cf} and CPE_{cf} , respectively. Additionally, W_0 represents the Warburg element for diffusion of lithium ions. The fitting results were shown in Table S1.† Note that the decrease of the R_{ct} with increasing charge/discharge cycles is in line with some reported studies with NiO-based electrodes. 22,24,73 The decrease of the charge transfer resistance can be attributed to the feasibility of the charge transfer for the following cycles after the activation process is initially presented.⁷⁴ The specific capacity gradually decreased to 809 mA h g⁻¹ after 1000 cycles, which was still 2.2 times higher than that of the graphite anode (372 mA h g⁻¹). The specific capacity retention after 1000 cycles was 73% and the average coulombic efficiency reached 99.86%. The cycling performance of the Ni/NiO/C composite materials with sheet-film morphology was collected for comparison. The long cycle tests showed that the sheet-film Ni/ NiO/C anode was subject to a sudden capacity loss at the 187th cycle (Fig. S11c†). Such an abrupt capacity loss may be attributed to the loss of electrical contact with the current collector, which is commonly observed during the pulverization of electrode materials. It is therefore evident that the sheet-film Ni/NiO/C anode

15

20

30

35

40

45

50

55

cannot mitigate the volume change issues of the nickel oxide based conversion reaction type anode. The TEM image (Fig. S14†) of the nanoporous gyroid Ni/NiO/C nanocomposite after 1000 cycles showed that the original morphology of the electrode materials was preserved, indicating a high stability of the active materials in LIBs. As expected, by taking advantage of the unique network nanostructure, those nanoporous gyroid Ni/NiO/C nanocomposite anodes manifest high specific capacity and long-term cycling stability. We have compared this with the cycling performance with previous reported NiO based anodes (see ESI, Table S2†), and the gyroid Ni/NiO/C nanocomposite is among one of the most stable anodes.

4 Conclusions

10

15

35

55

In conclusion, a nanoporous gyroid Ni/NiO/C nanocomposite with a well-ordered nanonetwork texture was successfully fabricated and developed as an electrode in the LIB applications. Following the fabrication of gyroid-structured PS/Ni nanohybrids with templated electroless plating of Ni using nanoporous PS from a self-assembled degradable BCPs template, a calcination process to generate the PS template and

oxidize Ni was performed. The Ni/NiO composite with a well-preserved gyroid texture was used for carbon coating and produced a nanoporous gyroid Ni/NiO/C nanocomposite that was further evaluated as an anode material for LIBs. Benefiting from the well-interconnected nanoporous structure with an ultrafine transition metal oxide nanonetwork and uniform carbon coating, the gyroid Ni/NiO/C electrodes exhibited excellent specific capacity, ratability and cyclability. This work demonstrates the great potential of the Ni/NiO/C nanocomposite with well-ordered nanonetwork textures in the design of high power LIBs. It is appealing to exploit the suggested approaches for the design and the development of high-rate capability electrodes in the future.

Conflicts of interest

The authors declare no competing financial interest.

Acknowledgements

The authors acknowledge Dr B. Wang and Dr M. Gao for the help with the SEM and TEM. The SEM observations using Quanta450 were carried out at the Liquid Crystal Institute Characterization Facility of Kent State University. The authors are grateful for financial support from The University of Akron.

This work is supported by the National Science Foundation (NSF-CBET1505943, 1706681 and NSF-DMR1554851) and Ohio Federal Network Research (OFRN).

References

1 A. S. Arico, P. Bruce, B. Scrosati, J.-M. Tarascon and W. V. Schalwkijk, *Nat. Mater.*, 2005, 4, 366–377.

2 M. R. Gao, Y. F. Xu, J. Jiang and S. H. Yu, *Chem. Soc. Rev.*, 2013, 42, 2986–3017.

- 3 K. Naoi, S. Ishimoto, J.-I. Miyamoto and W. Naoi, *Energy Environ. Sci.*, 2012, 5, 9363–9373.
- 4 Y.-G. Guo, J.-S. Hu and L.-J. Wan, *Adv. Mater.*, 2008, **20**, 2878–2887.
- 5 C. Liu, F. Li, L. P. Ma and H. M. Cheng, *Adv. Energy Mater.*, 2010, **22**, E28.
- 6 M. D. Stoller, S. Park, Ysif. 3c Zhu, J. An and R. S. Ruoff, *Nano Lett.*, 2008, **10**, 3498–3502.
- 7 B. Dunn, H. Kamath and J.-M. Tarasco, *Science*, 2011, 334, 928–935.
- 8 K. Kang, Y. S. Meng, J. Breger, C. P. Grey and G. Ceder, *Science*, 2006, 311, 977–980.
- 9 J. B. Goodenough and Y. Kim, *Chem. Mater.*, 2010, 22, 587-603
- 10 S. Liu, Z. Wang, C. Yu, H. B. Wu, G. Wang, Q. Dong, J. Qiu, A. Eychmuller and X. W. Lou, *Adv. Mater.*, 2013, 25, 3462– 3467
- 11 L. Qie, W. M. Chen, Z. H. Wang, Q. G. Shao, X. Li, L. X. Yuan, X. L. Hu, W. X. Zhang and Y. H. Huang, *Adv. Mater.*, 2012, **24**, 2047–2050.
- 12 Y. Yu, C. Yan, L. Gu, X. Lang, K. Tang, L. Zhang, Y. Hou, Z. Wang, M. W. Chen, O. G. Schmidt and J. Maier, *Adv. Energy Mater.*, 2013, 3, 281–285.
- 13 L. Zhang, H. B. Wu, B. Liu and X. W. Lou, *Energy Environ. Sci.*, 2014, 7, 1013–1017.
- 14 K. Cao, L. Jiao, H. Liu, Y. Liu, Y. Wang, Z. Guo and H. Yuan, *Adv. Energy Mater.*, 2015, 5, 1401421.
- 15 M. V. Reddy, G. V. SubbaRao and B. V. Chowdari, *Chem. Rev.*, 2013, **113**, 5364–5475.
- 16 Y. Sun, X. Hu, W. Luo, F. Xia and Y. Huang, *Adv. Funct. Mater.*, 2013, 23, 2436–2444.
- 17 C. He, S. Wu, N. Zhao, C. Shi, E. Liu and J. Li, *ACS Nano*, 2013, 7, 4459–4469.
- 18 B. Jiang, Y. He, B. Li, S. Zhao, S. Wang, Y.-B. He and Z. Lin, *Angew. Chem., Int. Ed.*, 2017, **56**, 1869–1872.
- 19 B. Jiang, C. Han, B. Li, Y. He and Z. Lin, *ACS Nano*, 2016, **10**, 2728–2735.
- 20 J. Liang, H. Hu, H. Park, C. Xiao, S. Ding, U. Paik and X. W. Lou, *Energy Environ. Sci.*, 2015, **8**, 1707–1711.
- 21 F. Zou, Y. M. Chen, K. Liu, Z. Yu, W. Liang, S. M. Bhaway, M. Gao and Y. Zhu, *ACS Nano*, 2016, **10**, 377–386.
- 22 X. Sun, W. Si, X. Liu, J. Deng, L. Xi, L. Liu, C. Yan and O. G. Schmidt, *Nano Energy*, 2014, **9**, 168–175.
- 23 W. Guo, W. Sun and Y. Wang, ACS Nano, 2015, 9, 11462-11471.
- 24 X. Sun, C. Yan, Y. Chen, W. Si, J. Deng, S. Oswald, L. Liu and O. G. Schmidt, *Adv. Energy Mater.*, 2014, **4**, 1300912.
- 25 S. Zhao, Z. Wang, Y. He, B. Jiang, Y. Harn, X. Liu, F. Yu, F. Feng, Q. Shen and Z. Lin, ACS Energy Lett., 2017, 2, 111–116.
- 26 Z. Gong and Y. Yang, Energy Environ. Sci., 2011, 4, 3223–3242.
- 27 P. Roy and S. K. Srivastava, *J. Mater. Chem. A*, 2015, **3**, 2454–2484.
- 28 P. G. Bruce, B. Scrosati and J. M. Tarascon, *Angew. Chem., Int. Ed.*, 2008, 47, 2930–2946.
- 29 L. Ji, Z. Lin, M. Alcoutlabi and X. Zhang, *Energy Environ. Sci.*, 2011, 4, 2682–2699.

10

15

20

25

30

35

40

45

- 30 Y. Kim, J.-H. Lee, S. Cho, Y. Kwon, I. In, J. Lee, N.-H. You, E. Reichmanis, H. Ko, K.-T. Lee, H.-K. Kwon, D.-H. Ko, H. Yang and B. Park, *ACS Nano*, 2014, **8**, 6701–6712.
 - 31 Z.-S. Wu, G. Zhou, L.-C. Yin, W. Ren, F. Li and H.-M. Cheng, *Nano Energy*, 2012, 1, 107–131.
 - 32 Z. Wang, D. Luan, S. Madhavi, Y. Hu and X. W. Lou, *Energy Environ. Sci.*, 2012, **5**, 5252–5256.
 - 33 F. Zou, X. Hu, L. Qie, Y. Jiang, X. Xiong, Y. Qiao and Y. Huang, *Nanoscale*, 2014, **6**, 924–930.
- 34 J. M. Jeong, B. G. Choi, S. C. Lee, K. G. Lee, S. J. Chang, Y. K. Han, Y. B. Lee, H. U. Lee, S. Kwon, G. Lee, C. Lee and Y. Huh, *Adv. Mater.*, 2013, 25, 6250–6255.
 - 35 Z. Fan, J. Liang, W. Yu, S. Ding, S. Cheng, G. Yang, Y. Wang, Y. Xi, K. Xi and R. V. Kumar, *Nano Energy*, 2015, **16**, 152–162.
- 36 H. Zhang, T. Shi, D. J. Wetzel, R. G. Nuzzo and P. V. Braun, Adv. Mater., 2016, 28, 742–747.
 - 37 X. Pang, Y. He, J. Jung and Z. Lin, Science, 2016, 353, 1268-1272.
 - 38 X. Pang, L. Zhao, W. Han, X. Xin and Z. Lin, *Nat. Nanotechnol.*, 2013, **8**, 426–431.
 - 39 F. S. Bates and G. H. Fredrickson, *Annu. Rev. Phys. Chem.*, 1990, **41**, 525–557.
 - 40 F. S. Bates and G. H. Block Fredrickson, *Phys. Today*, 1999, **52**, 32–40.
- 41 A. S. Zalusky, R. O. Valles, C. J. Taylor and M. A. Hillmyer, J. Am. Chem. Soc., 2001, 123, 1519–1520.
 - 42 W. H. Tseng, C. K. Chen, Y. W. Chiang, R. M. Ho, S. Akasaka and H. Hasegawa, *J. Am. Chem. Soc.*, 2009, **131**, 1356–1357.
 - 43 Y. T. Tseng, W. H. Tseng, C. H. Lin and R. M. Ho, *Adv. Mater.*, 2007, **19**, 3584–3588.
 - 44 M. Park, C. Harrison, P. M. Chaikin, R. A. Register and D. H. Adamson, *Science*, 1997, 276, 1401–1404.
 - 45 T. T. Albrecht, R. Steiner, J. DeRouchey, C. M. Stafford, E. Huang, M. Bal, M. Tuominen, C. J. Hawker and T. P. Russell, *Adv. Mater.*, 2000, **12**, 787–791.
 - 46 J. Y. Cheng, C. A. Ross, V. Z. H. Chan, E. L. Thomas, R. G. H. Lammertink and G. J. Vancso, *Adv. Mater.*, 2001, 13, 1174–1178.
 - 47 T. C. Lin, K. C. Yang, P. Georgopanos, A. Avgeropoulos and R. M. Ho, *Polymer*, 2017, **126**, 360–367.
 - 48 H. Y. Hsueh, C. T. Yao and R. M. Ho, *Chem. Soc. Rev.*, 2015, 44, 1974–2018.
 - 49 S. Grimm, R. Giesa, K. Sklarek, A. Langner, U. Gosele, H.-W. Schmidt and M. Steinhart, *Nano Lett.*, 2008, **8**, 1954–1959.
 - 50 F. Li, X. Yao, Z. Wang, W. Xing, W. Jin, J. Huang and Y. Wang, *Nano Lett.*, 2012, **12**, 5033–5038.
 - 51 E. J. W. Crossland, M. Kamperman, M. Nedelcu, C. Ducati, U. Wiesner, D. M. Smilgies, G. E. S. Toombes,

- M. A. Hillmyer, S. Ludwigs, U. Steiner and H. J. Snaith, *Nano Lett.*, 2009, **9**, 2807–2812.
- 52 S. Guldin, I. Rushkin, M. Stefik, K. Hur, U. Wiesner, J. J. Baumber and U. Steiner, Adv. Mater., 2011, 23, 3664– 3668
- 53 M. R. J. Scherer, L. Li, P. M. S. Cunha, O. A. Scherman and U. Steiner, *Adv. Mater.*, 2012, **24**, 1217–1221.
- 54 H. Y. Hsueh, Y. C. Huang, R. M. Ho, C. H. Lai, T. Makida and H. Hasegawa, *Adv. Mater.*, 2011, 23, 3041–3046.
- 55 H. Y. Hsueh, H. Y. Chen, Y. C. Hung, Y. C. Ling, S. J. Gwo and R. M. Ho, *Adv. Mater.*, 2013, **25**, 1780–1786.
- 56 C. F. Cheng, H. Y. Hsueh, C. H. Lai, C. J. Pan, B. J. Hwang, C. C. Hu and R. M. Ho, NPG Asia Mater., 2015, 7, e170.
- 57 K. W. Liu, Y. M. Chen, G. M. Policastro, M. L. Becker and Y. Zhu, *ACS Nano*, 2015, **9**, 6041–6049.
- 58 H. Y. Hsueh, H. Y. Chen, M. S. She, C. K. Chen, R. M. Ho, S. J. Gwo, H. Hasegawa and E. L. Thomas, *Nano Lett.*, 2010, 10, 4994–5000.
- 59 H. Y. Hsueh and R. M. Ho, *Langmuir*, 2012, **28**, 8518–8529.
- 60 Y. Wan and D. Zhao, Chem. Rev., 2007, 107, 2821-2860.
- 61 J. Bella, R. Yeb, K. Ahmedc, C. Liu, M. Ozkanc and C. S. Ozkana, *Nano Energy*, 2015, **18**, 47–56.
- 62 H. Y. Hsueh, Y. C. Ling, H. F. Wang, L. Y. C. Chien, Y. C. Hung, E. L. Thomas and R. M. Ho, *Adv. Mater.*, 2014, **26**, 3225–3229.
- 63 F. Zou, X. Hu, Y. Sun, W. Luo, F. Xia, L. Qie, Y. Jiang and Y. Huang, *Chem.–Eur. J.*, 2013, **19**, 6027–6033.
- 64 A. N. Mansour, Surf. Sci. Spectra, 1994, 3, 231-248.
- 65 A. N. Mansour, Surf. Sci. Spectra, 1994, 3, 239-246.
- 66 H. Wang, X. Fan, X. Zhang, Y. Huang, Q. Wu, Q. Pana and Q. Li, *RSC Adv.*, 2017, 7, 23328–23333.
- 67 D. T. Dam, X. Wang and J.-M. Lee, ACS Appl. Mater. Interfaces, 2014, 6, 8246–8256.
- 68 M. A. Peck and M. A. Langell, *Chem. Mater.*, 2012, **24**, 4483–4490.
- 69 W. Liu, C. Lu, X. Wang, K. Liang and B. K. Tay, *J. Mater. Chem. A*, 2015, 3, 624–633.
- 70 G. Zhou, D.-W. Wang, L.-C. Yin, N. Li, F. Li and H.-M. Cheng, *ACS Nano*, 2012, **6**, 3214–3223.
- 71 X. Zheng, H. Wang, C. Wang, Z. Deng, L. Chen, Y. Lia, T. Hasan and B.-L. Su, *Nano Energy*, 2016, 22, 269.
- 72 C. Peng, B. Chen, Y. Qin, S. Yang, C. Li, Y. Zuo, S. Liu and J. Yang, *ACS Nano*, 2012, **6**, 1074–1081.
- 73 G. Huang, X. Guo, X. Cao, Q. Tian and H. Sun, *Nano Energy*, 2016, **28**, 338–345.
- 74 B. Yan, M. Li, X. Li, Z. Bai, L. Dong and D. Li, *Electrochim.Acta*, 2015, **164**, 55–61.

55

20

30

35

40

45

50

55